ELSEVIER

Journal of Marine Systems 21 (1999) 67–84

JOURNAL OF MARINE SYSTEMS

Comparison of dissipation of turbulent kinetic energy determined from shear and temperature microstructure

O. Kocsis [a], H. Prandke [b], A. Stips [c], A. Simon [a], A. Wüest [a,*]

[a] *Swiss Federal Institute of Environmental Science and Technology (EAWAG) and Swiss Federal Institute of Technology (ETH), CH-8600 Dübendorf, Switzerland*

[b] *ISW In Situ Wassermesstechnik, Lenzerstrasse 5, D-17213 Petersdorf, Germany*

[c] *CEC-JRC ISPRA, Space Applications Institute, Marine Environment Unit, I-21020 Ispra (VA) TP272, Italy*

Received 14 November 1997; accepted 20 July 1998

Abstract

A total of 826 temperature and shear microstructure profiles, measured during 12 days in March 1996 in Lake Neuchâtel (Switzerland), are used to compare estimates of turbulent kinetic energy dissipation, determined by the Batchelor (μT; temperature) and the dissipation (μS; shear) methods. Positioned horizontally 35 m apart, the two different profilers were raised through the nearly-homogeneous surface boundary layer. The collected time series covered different atmospheric forcings, including calm (≈ 1 m s^{-1}) and windy (>10 m s^{-1}) periods, as well as periods of thermally-induced convection (nights) and stratification (sunny days). Consequently, dissipation varied over 6 orders of magnitudes from 10^{-11} to 10^{-5} W kg^{-1}. The comparison of the 72′674 pairs of dissipation estimates, determined from 25 cm long vertical profile segments, reveals excellent agreement for the bulk of the estimates, with deviations smaller than a factor of 2. In a relatively small subset, collected under strong heating, deviations of up to a factor of 6 occur in 1–4 m depth. These deviations are, however, just about within the 95% confidence limits of the bootstrap distribution. Under low turbulence the μT method tends to provide slightly larger dissipation, whereas for high wind-induced turbulence the μS method gives larger dissipation.

Keywords: turbulent mixing; lakes; temperature microstructure; shear microstructure; dissipation

1. Introduction

The vertical and cross-isopycnal (diapycnal) turbulent fluxes of heat, salt, density and biogeochemical compounds are central to the hydrodynamics and the ecology of stratified natural waters such as oceans, lakes and reservoirs. A key quantity for the description of turbulent mixing is the rate of dissipation ε [W kg^{-1}] of turbulent kinetic energy (TKE) for three reasons: (1) ε is considered to be a direct measure of the production of TKE, since the rate of storage of potential energy is generally small compared to the sources and sinks of TKE; (2) ε can be compared directly to the output of turbulence models balancing TKE (Sander, 1998); and (3) ε can be used for estimating diapycnal diffusivity by applying the Osborn (1980) approach

$$K_d = \gamma_{mix}\,\varepsilon N^{-2} \qquad [\mathrm{m^2\ s^{-1}}] \qquad (1)$$

* Corresponding author. EAWAG, CH-8600 Dübendorf, Switzerland. Fax: +41-1-823-52-10; E-mail: wuest@eawag.ch

0924-7963/99/$ - see front matter
PII: S0924-7963(99)00006-8

where γ_{mix} [−] denotes the mixing efficiency; $N^2 = -g\rho^{-1}\partial\rho/\partial z$ [s^{-2}] is the stability of the water column; g [m s^{-2}] is the acceleration due to gravity; ρ [kg m^{-3}] is the pressure-independent density and z [m] the vertical coordinate (positive upwards).

Among the methods to determine the dissipation of TKE in stratified natural waters, two microstructure techniques have become common (Gregg, 1991). The *dissipation method* is based on measured records of small-scale shear fluctuations $\partial u'/\partial z$. The assumption of isotropy allows dissipation to be determined by using $\varepsilon = 7.5\nu\langle(\partial u'/\partial z)^2\rangle$ (Osborn, 1980), where ν denotes the kinematic viscosity of water ($1–1.5 \times 10^{-6}$ m^2 s^{-1}). The *Batchelor method* is based on profiles of microstructure temperature fluctuations (Batchelor, 1959), which allow temperature power spectra ϕ_T [K^2 $(cpm)^{-1}$] to be computed from profile segments (cpm = cycle per meter). Dissipation is determined by fitting the spectra to Batchelor's model spectrum (Gibson and Schwarz, 1963; Dillon and Caldwell, 1980). As both methods require several assumptions about the intrinsic structure of turbulence at small scales, the two methods do not necessarily yield the same dissipation ε. In the following, the *dissipation method* (shear microstructure) and the Batchelor method (temperature microstructure) will be abbreviated by μS and μT, respectively.

Since for economic reasons oceanic microstructure measurements are usually done with fast profiling shear probes, only few intercomparison studies, using the same profiler, have been made. Oakey (1982) used a very fast response DISA thin-film thermometer (time constant 2×10^{-3} s, resolution 2×10^{-4} K, disadvantage of noise) in order to attain an adequate spatial resolution for the temperature microstructure fluctuations. Using data segments of 10–15 m length, he found that the 25 values of ε, calculated simultaneously from the high wavenumber spectra of temperature and velocity shear, agreed to within a factor of 2 in the rather narrow range of 5×10^{-9} to 5×10^{-7} W kg^{-1}.

The comparison by Oakey (1982) is not the only in situ validation of microstructure dissipation measurements. Since the main purpose of the microstructure method is the estimation of local diapycnal diffusivity K_d in stratified waters (Eq. (1)), there has been a need to compare microstructure measurements with diffusivity determined by other means. The motivation for this study was the fact that both the Batchelor method (Davis, 1993; Davis, 1994) and the dissipation method (Gregg, 1989) yield diffusivities in the ocean thermocline which are an order of magnitude smaller than those found by matching basin-wide observations to models or tracer budgets. Ledwell et al. (1993) resolved this seeming paradox by demonstrating that mixing felt by passive tracer in the interior of the thermocline is indeed as low as that revealed by microstructure measurements. Simultaneous tracer and microstructure measurements in lakes have also clearly shown the equivalence of tracer and microstructure diffusivity estimates (Wüest et al., 1996; Goudsmit et al., 1997).

Comparisons between different microstructure profilers, simultaneously collecting data close to each other are rare. Such an investigation was carried out by Moum et al. (1995) in the top 350 m of the equatorial ocean. Almost 1000 μS shear profiles were collected by the Oregon State University and APL (University of Washington) groups who operated within a distance of 11 km of each other during 3.5 days. As a result, the two overall bin-averaged vertical profiles of ε estimates agree generally within a factor of 2 with no systematic bias and only a few averages disagree by more than the 95% confidence interval, determined by the bootstrap method. Occasionally hourly averages of ε differed by several factors of 10: the reason is believed to be natural variability (so-called intermittency) of ε, which ranged from 10^{-10} to 10^{-5} W kg^{-1} (Moum et al., 1995).

The scope of this publication is to compare the dissipation estimates determined by the two completely different approaches using temperature and shear microstructure data. The two profilers were run upward simultaneously but independently within a horizontal distance of 35 m of each other in the top 30 m of Lake Neuchâtel. This comparison, aimed at evaluating the uncertainties in the estimation of ε, is of interest for two reasons. (1) The differences in methods, experimental configurations, sensor behavior, and analogue and digital processing may lead to deviations on purely technical grounds. (2) Some reservations exist with respect to the Batchelor method, since non-turbulent (fossil) remnant temperature structure may affect the spectra obtained, and

since temperature spectra of limited segment length do not necessarily follow the Batchelor form (Sherman and Davis, 1995). Several differences exist between the Oakey (1982) investigation and this study: (1) The μS and μT sensors did not sample the identical water column, since we employed two different profilers (Fig. 1a). (2) We collected a much larger set of data, allowing 826 profiles and 72′674 individual ε estimates, respectively, to be compared. (3) In addition, the observed ε values of 10^{-11}–10^{-5} W kg^{-1} varied over four orders of magnitude more than those by Oakey ($\approx 5\times10^{-9}$ to 5×10^{-7} W kg^{-1}). (4) The 0.25 m segmentation of the microstructure profiles was $\approx$40 times shorter than that of Oakey's, since we aimed to resolve the vertical structure of the surface boundary layer.

The comparison of the two data sets represents the core of this paper. The two measurement techniques, the profilers and data analysis are explained in Section 2, with further details given in Appendix A. The location of the experiment (the weakly stratified surface layer of Lake Neuchâtel, Switzerland), the details of the experimental set-up, and the overall meteorological forcing are described in Section 3. The dynamics of the turbulent response for the 12-day measurement period and the statistical comparison of the two data sets is discussed in Section 4. Conclusions related to the consistency and discrepancy of the two methods are drawn in Section 5.

2. Microstructure methods and employed profilers

2.1. Batchelor method

The Batchelor method is based on the fact that small-scale temperature fluctuations are always pre-

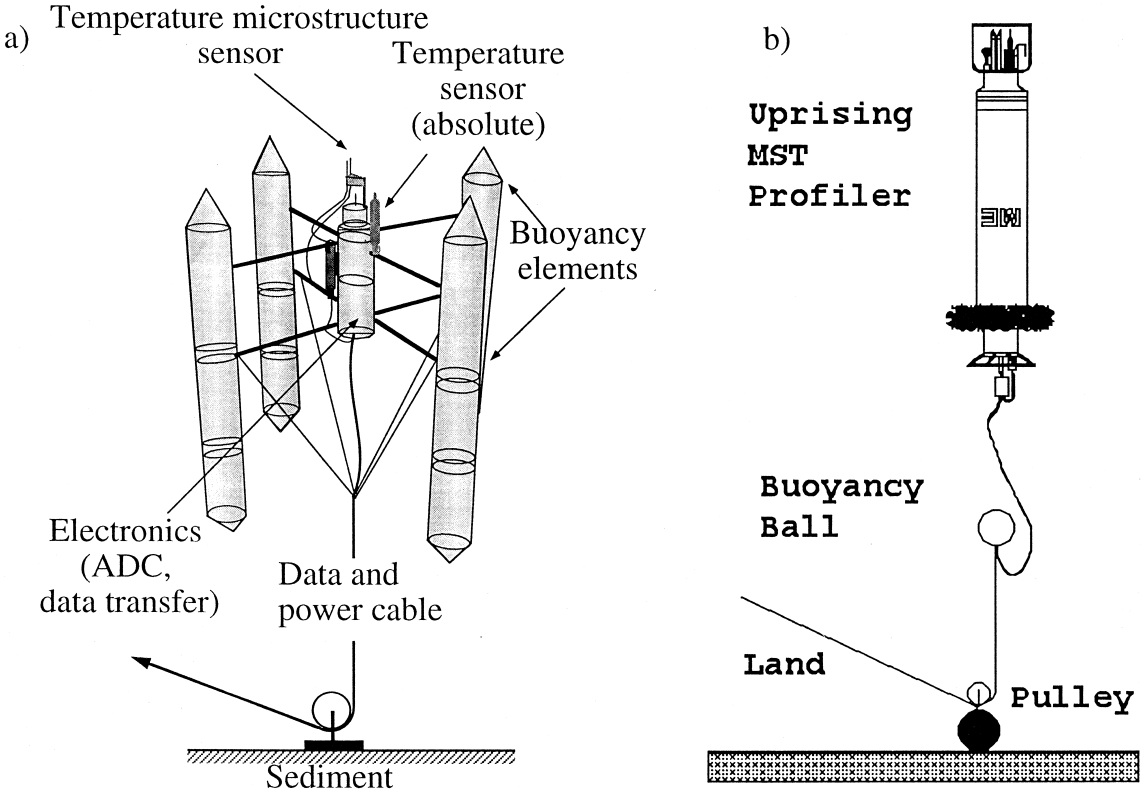

Fig. 1. Schematic illustration of the μT (a) and μS (b) microstructure profilers, respectively, operated in uprising mode using a winch at the land station. See technical details in Appendix A.

sent in natural waters. The relationship between the temperature fluctuations at the smallest length scales (≈ mm)—where temperature differences are smoothed by thermal diffusivity κ_T—and the intensity of turbulent mixing is described by the Batchelor (1959) theory. Under isotropic and stationary conditions, the spectrum of one-dimensional temperature fluctuations follows the form:

$$\phi_T(k_z) = \frac{\pi\chi\kappa_T^{1/2}q^{3/2}\upsilon^{3/4}}{\varepsilon^{3/4}} \times\left(\frac{e^{-x^2}}{x} - \sqrt{\pi}(1-\mathrm{erf}(x))\right) \quad \left[K^2\ (\mathrm{cpm})^{-1}\right] \qquad (2)$$

where k_z [cpm] denotes the one-dimensional wavenumber, $x = 2\pi k_z \kappa_T^{1/2}\upsilon^{1/4}q^{1/2}\varepsilon^{-1/4}$ (the non-dimensional wavenumber), and $q = 3.4$ is the experimentally determined turbulence parameter (Grant et al., 1968; Dillon and Caldwell, 1980; Oakey, 1982; Imberger and Boashash, 1986). Since the constancy of q has been questioned by Gargett, 1985 (see Peters et al., 1988), the comparison of the differently determined ε estimates is of even more interest. Rates of dissipation of TKE, ε, and of temperature variance, χ [$K^2\ s^{-1}$], are determined by fitting the spectra of measured temperature profiles to the Batchelor (1959) model spectrum (Eq. (2)).

Temperature microstructure data were collected at 96 Hz from a FP07 fast response thermistor (nominal response time $\tau_{Resp} \approx 7\times10^{-3}$ s; relative resolution $\approx 10^{-4}$ K) using an adapted SBE-9 CTD (SeaBird, Bellevue, USA; Fig. 1a) as μT profiler, rising to the lake surface at a speed of $w = 0.08$ m s^{-1}. Data were transmitted via electrical cable to a computer at the shore (details in Simon, 1997). To reduce quantization noise of the temperature fluctuations at small scales, preemphasis (Mudge and Lueck, 1994) was applied by linearly enhancing the microstructure signal (as a function of frequency) before 16 bit A/D conversion (details in Appendix A and Gloor et al., 1995). Response time correction and deemphasis (Appendix A) was applied to the calculated spectra before fitting Eq. (2) to $\phi_T(k_z)$. We assumed a speed-dependent response time of the FP07 sensor of $\tau_{Resp} \approx (w/1\ ms^{-1})^{-0.32}7\times10^{-3}$ s ($\approx 16\times10^{-3}$ s for $w = 0.08$ m s^{-1}), according to Gregg and Meagher (1980). Applying the formula provided by Vachon and Lueck (1984) would slightly increase the highest ε estimates. Temperature spectra, calculated from 0.25 m long vertical segments, which did not follow Batchelor's form (less than 10% of the spectra), were rejected for further analysis.

2.2. Dissipation method

The dissipation method allows to determine the rate of dissipation ε from measured vertical gradient profiles of the horizontal current fluctuations $\partial u'/\partial z$. Assuming isotropic turbulence, the dissipation

$$\varepsilon = 7.5\nu\left\langle\left(\frac{\partial u'}{\partial z}\right)^2\right\rangle = 15\nu\int_0^\infty \phi_s\,dk_z \qquad \left[W\ kg^{-1}\right] \qquad (3)$$

is determined by integrating the shear spectra $\phi_s(k_z)$ of the measured shear $\partial u'/\partial z$.

In this study, small-scale shear $\partial u'/\partial z$ was measured using a 1-m long μS profiler (ME Meerestechnik-Elektronik, Trappenkamp, Germany, Fig. 1b) equipped with a PNS 93 shear sensor (Appendix A) and a profiler-internal vibration sensor (Prandke and Stips, 1996). Balanced with adjustable weights, the μS profiler was rising at a speed of $w = 0.35$ m s^{-1}. Sensor output was sampled at 1000 Hz, digitized by 16-bit A/D conversion and finally transmitted via electric cable to a computer at the shore (details in Prandke and Stips, 1996).

To suppress high and low frequency disturbances, the raw shear profile was filtered using a non-recursive digital bandpass filter (Walraven, 1984), ranging from 2 cpm to $k_K/2$, where $k_K = (2\pi)^{-1}(\varepsilon/\nu^3)^{1/4}$ is the Kolmogorov wavenumber (Prandke and Stips, 1996). As k_K is a function of ε, the upper boundary was iteratively adjusted until ε converged (Moum et al., 1995). The preliminary ε estimate, determined by using the summation method, allowed us to calculate and add the lost variance below 2 cpm (ε-dependent). In order to correct for the 14% of unresolved variance above $k_K/2$, ε was finally multiplied by 1.16 ($= 0.86^{-1}$).

The lower limit of reliable dissipation estimates depends on the rising velocity w of the shear sensor and profiler vibrations. For upward profiling, as in Lake Neuchâtel, the lower limit is about 10^{-10} W

kg^{-1}, as determined in a lake during extremely quiet conditions (Prandke and Stips, 1998). The small size of the airfoil of the PNS 93 sensor (3.5 mm length) allows dissipation estimates as high as 10^{-4} W kg^{-1} without correction for unresolved spectral content at the high wavenumber end.

3. Experiment

3.1. Experimental setup

The main goal of the turbulence measurements in Lake Neuchâtel was to quantify and parameterize wind-driven surface boundary layer turbulence (Simon, 1997; Simon et al., 1999). In this context, the comparison between the two microstructure techniques is a deliberate by-product. Such profiles from lake surface layers are ideal for this comparison, since dissipation may span a wide range of values as a function of depth and time, if variations of atmospheric forcing is strong and fast. This should allow a comparison of the two methods over a wide range of dissipation. In addition those variations due to changing external forcing, turbulence shows a high degree of inherent variability (typically ≈ 2 orders of magnitude), so-called intermittency (Baker and Gibson, 1987). Therefore, long data sets are necessary in order to get mean values with adequate levels of confidence.

Lake Neuchâtel, located in the western part of Switzerland (46°53′N; 6°47′E), was chosen as the experimental site, since it sees strong and highly variable wind forcing. In addition, the lake is wide and deep enough to ensure, that the influence of the lake boundaries on the physics of the surface boundary layer of the open water is negligible and that the fetch is long enough to allow waves to become fully developed. The quasi rectangular lake has maximum length, maximum width, maximum depth and mean depth of ≈ 38 km, ≈ 6 km, 153 m and 64 m, respectively. The location for the experiment (Chez-Le-Bart), shown in Fig. 2, was selected for its wind exposure and steep shore line. This location enables the operation of the two microstructure profilers (μS and μT), deployed about 300 m away from the shore at a local depth of ≈ 40 m, from a land station. The two profilers were separated (horizontally) by 35 m to ensure safe mooring operations. The setup of all anchored instruments is depicted in the map of Fig. 2.

Microstructure profiles were taken in the top 30 m during 250 h between March 9 and 20, 1996, at a sampling interval of ≈ 15 min leading to a data set of 966 temperature and 1116 shear microstructure casts. For the comparison, only those 826 dissipation

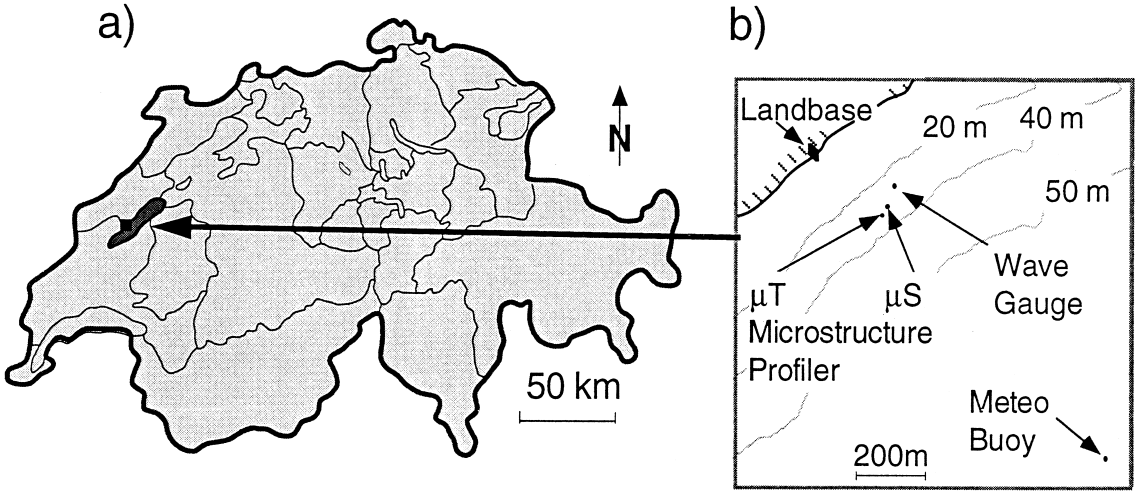

Fig. 2. (a) Location of Lake Neuchâtel (Switzerland) and (b) location of the experiment in March 1996 at the northwest coast. The positions of the microstructure profilers, the meteo station and the wave gauche are indicated.

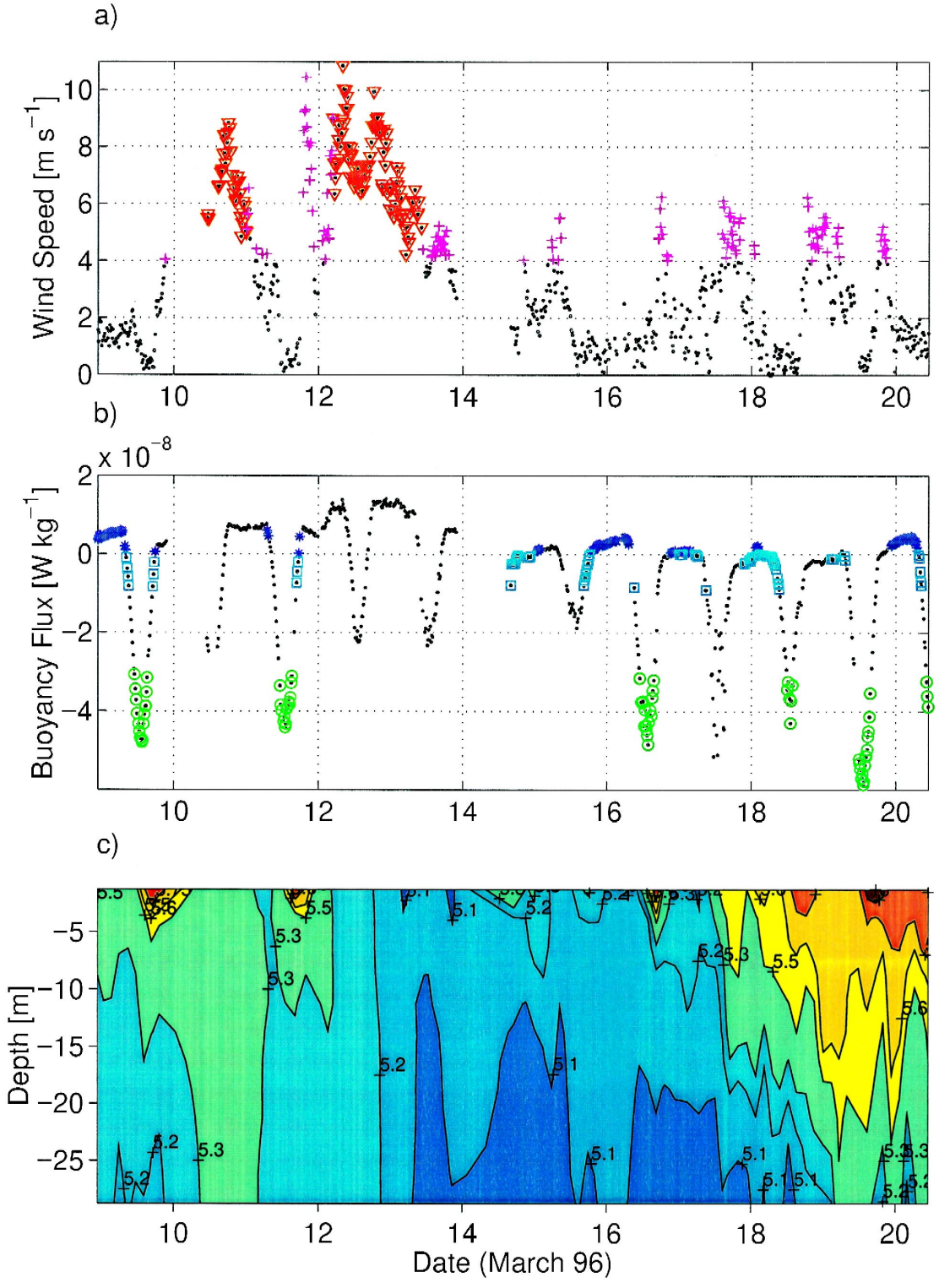
a)
Wind Speed [m s^{-1}]
0
2
4
6
8
10
10
12
14
16
18
20
b)
x 10^{-8}
Buoyancy Flux [W kg^{-1}]
2
0
−2
−4
10
12
14
16
18
20
c)
Depth [m]
−5
−10
−15
−20
−25
5.1
5.2
5.3
5.5
5.6
10
12
14
16
18
20
Date (March 96)

Table 1
Definition of the five mixing regimes, arbitrarily categorized for comparison

	Symbol	Wind [m s^{-1}]	Wave height $H_{1/3}$ [m]	Surface buoyancy flux J_b^0 [W kg^{-1}]	Number of profiles[a]
1	W, ∇	strong wind, ($w_{2.8} > 4$)	waves, ($H_{1/3} > 0.2$)	–	138
2	WN, +	strong wind, ($w_{2.8} > 4$)	no waves, ($H_{1/3} < 0.2$)	–	127
3	CON, *	weak wind, ($w_{2.8} < 2$)	–	TKE-producing[b] ($J_b^0 > 0$)	130
4	CA, □	weak wind, ($w_{2.8} < 2$)	–	weak TKE-suppressing[b] ($-1 \times 10^{-8} < J_b^0 < 0$)	80
5	SH, ○	weak wind, ($w_{2.8} < 2$)	–	strong TKE-suppressing[b] ($J_b^0 < -3 \times 10^{-8}$)	77

[a] From the total of 826 profiles included in the comparison 552 were assigned in one of the five mixing regimes according to the definitions.
[b] Surface buoyancy flux J_b^0 is defined as positive ($J_b^0 > 0$) for turbulence-producing conditions (convection) and negative ($J_b^0 < 0$) for turbulence-suppressing conditions (heating).

profiles were used which were measured within the same 15 min. Excluding segments with poorly-shaped Batchelor spectra or vibrations led finally to a data set for comparison of 72′674 individual dissipation estimates.

3.2. Meteorological background

Atmospheric forcing and the temperature-dependent water density stratification were studied during the experiment since both affect dissipation in the surface boundary layer. The meteorological conditions were measured on a meteo buoy, moored about 2000 m off the coast (Fig. 2). The sensors (Aanderaa Instruments, Bergen, Norway) were mounted 2.8 m above lake surface. Significant wave height $H_{1/3}$ and wave peak frequency f_p were monitored with a pressure sensor, moored in 1 m water depth (Fig. 2). Both microstructure profilers were equipped with a precision temperature sensor (Pt 100) for the absolute measurement of the background temperature profile with an accuracy of 10^{-3}°C allowing the development of the temperature stratification to be monitored.

The period between March 10 and 13 is characterized by strong winds (maximum 10-min average: 14.6 m s^{-1}) from NNE (Fig. 3a). Due to the long fetch, waves were generated with heights up to $H_{1/3} = 0.6$ m. After March 14 winds were of short duration only (usually 1 h). Since wind direction was predominantly NNW, wave activity was low ($H_{1/3} < 0.2$ m). The second part of the measurement period is characterized by strong warming (with a net average heat flux $\langle H_{net}(\text{March 8–20})\rangle \approx 48$ W m^{-2}). Due to the low temperature (≈ 5.2°C), which was close to the temperature of maximum density (≈ 3.95°C), thermal expansivity and subsequently also the surface buoyancy flux was small ($J_b^0 = 10^{-9}$ to 10^{-8} W kg^{-1}, Fig. 3b). Therefore wind was the main TKE input to the lake for most of the experiment. Convection was the dominant production of turbulence only during the nights of March 8/9, 15/16 and 19/20, respectively (Fig. 3b).

During the entire experiment stratification in the top 30 m was very weak due to preceding winter cooling and the low thermal expansivity. The weak initial stability ($N^2 = 10^{-4}$ s^{-2}) at the beginning of data collection was destroyed by strong winds and cooling from March 10 to 13. After March 14, stratification again built up due to increasing solar heating (Fig. 3c).

These varying meteorological conditions enabled the comparison of the two sets of dissipation under different forcings. Therefore, we categorized the collected microstructure data into five different forcing regimes (definitions in Table 1) abbreviated by W (*W*ind with waves), WN (*W*ind, *N*o waves), CA (*CA*lm conditions), CON (*CON*vective conditions)

Fig. 3. (a) Wind speed measured 2.8 m above water surface by three anemometers. The two symbols indicate the regimes W (strong wind with waves; ▽) and WN (strong wind no waves; +). Regime definitions in Table 1. (b) Surface buoyancy flux J_b^0 ($J_b^0 > 0$ is defined as to cause turbulence production) calculated from the net heat flux. The three symbols indicate the regimes CON (weak wind; positive J_b^0; *), CA (weak wind; weak negative J_b^0; □) and SH (weak wind; strong negative J_b^0; ○). (c) Background temperature [°C] contoured with levels 5.1°, 5.2°, 5.3°, 5.5°, 5.75° and 6.0°, measured by the μT profiler.

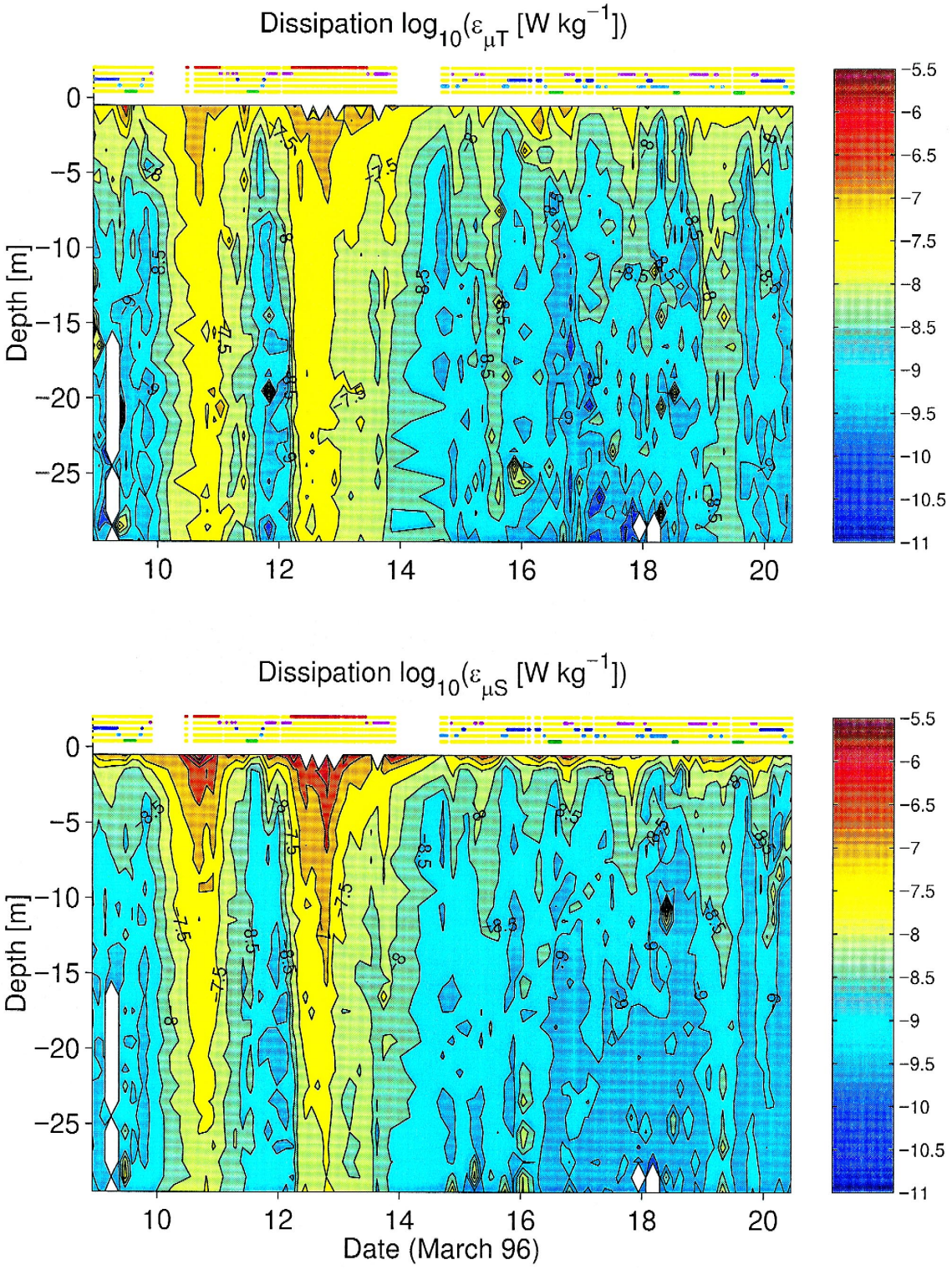
Dissipation $\log_{10}(\varepsilon_{\mu T}$ [W kg^{-1}])
Depth [m]
0
−5
−10
−15
−20
−25
10
12
14
16
18
20
−5.5
−6
−6.5
−7
−7.5
−8
−8.5
−9
−9.5
−10
−10.5
−11
Dissipation $\log_{10}(\varepsilon_{\mu S}$ [W kg^{-1}])
Depth [m]
Date (March 96)

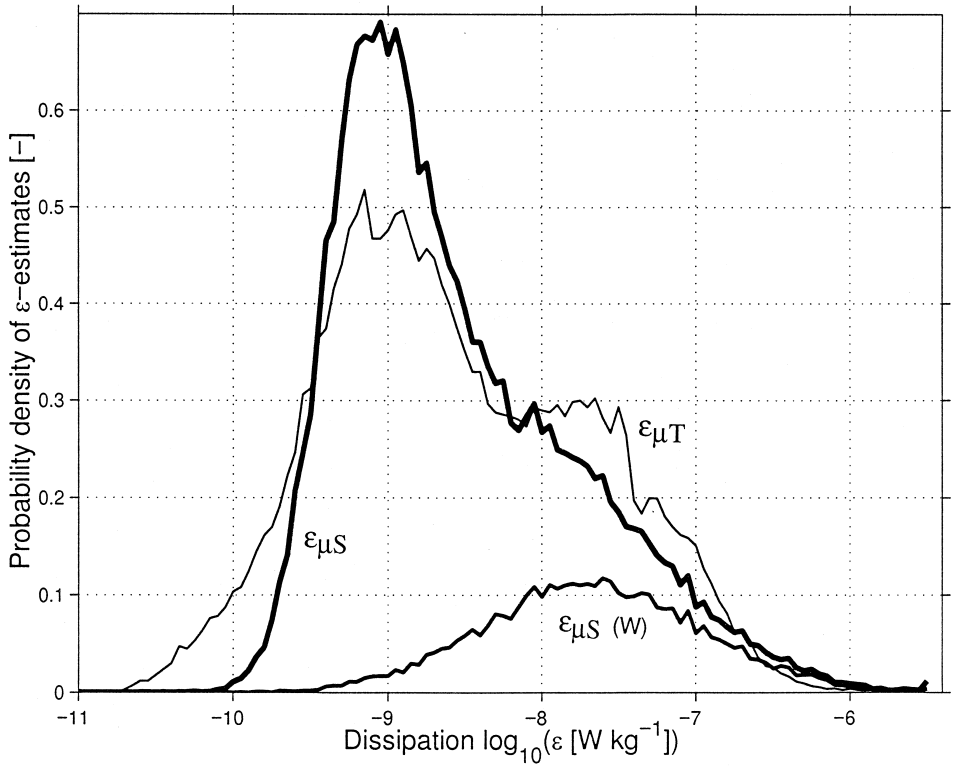

Fig. 5. Histograms of the entire data set of the 72′674 $\varepsilon_{\mu T}$ and $\varepsilon_{\mu S}$ values. The lower line shows the nearly lognormal histogram of the $\varepsilon_{\mu S}$ values from regime W (strong wind, Table 1).

and SH (*S*trong *H*eating). Wind speed (Fig. 3a) as well as surface buoyancy flux (Fig. 3b) are plotted in the same five color codes, as the categorization given at the tops of Fig. 4. From the 826 microstructure profiles, subject to the comparison, 552 profiles (number of profiles in Table 1) were included in this five categories.

4. Comparison of the dissipation estimates

The comparison of the dissipation estimates obtained by the μT and the μS methods, respectively, has to cope with the different factors influencing vertical and temporal variations of turbulence. Such factors are changing meteorological forcing and stratification, as well as intermittency. In a first step we present the entire set of ε estimates in a contour plot (Fig. 4), overviewing the temporal development of the dissipation profile during the 12 days of observation. In order to remove some of the intermittency of the 0.25-m based ε values, which individually vary over six orders of magnitude from 10^{-11} to 10^{-5} W kg^{-1}, dissipation has been averaged over 1 m and 2.5 h (up to 10 profiles) before contouring Fig. 4.

The temporal evolution of the two patterns of ε values shown in Fig. 4a (Batchelor method; μT) and in Fig. 4b (dissipation method; μS) coincide excellently. Agreement of the patterns refer to (1) the

Fig. 4. Contour plots of ε estimates, calculated from the 826 profiles of temperature ($\varepsilon_{\mu T}$, upper panel) and shear ($\varepsilon_{\mu S}$, lower panel) microstructure. Before plotting, ε values were averaged over 1 m and 2.5 h. White areas indicate missing data from either system. Contour levels are drawn at 0.5 decade intervals of the logarithmic dissipation $\log_{10}(\varepsilon$ [W kg^{-1}]). The five lines at the top of the plots correspond to the five selected regimes (Table 1, 1st column) and to the colors in Fig. 3a,b.

nearly identical absolute ε values, (2) the transitions of ε between turbulent and calm periods and (3) the vertical structure of ε. Since during most of the experiment turbulence was mainly determined by wind, dissipation increases towards the surface, revealing a more or less pronounced *law of the wall* layer below ≈ 1 m depth (Simon et al., 1999). In Fig. 4, most of the differences are within one level of the contour plot indicating deviations of smaller than a factor of $\sqrt{10} \approx 3.2$. Due to the intrinsic characteristics of turbulence, inherent to both methods, perfect agreement can not be expected, especially not for weak turbulence where intermittency becomes manifest. Disagreement on such scales of 1 m and ≈ 10 profiles (2.5 h) are therefore not of further interest for the comparison of the two methods.

More interesting are the deviations of systematic nature, which can potentially be found on averages over longer time scales. Fig. 4 reveal three deviations: Firstly, in the top surface layer, where dissipation increases towards the surface, it turns out that the increase is stronger for $\varepsilon_{\mu S}$ than for $\varepsilon_{\mu T}$ by up to an order of magnitude during strong wind (regime W), especially in the top ≈ 1–2 m. Secondly, a deviation was identified for the period of strong heating (regime SH) in the depth range of 1–4 m. The third apparent deviation can be found at the end of the observation period (after March 17) parallel to the increase of stratification in 15–20 m depth (Fig. 3c), where turbulence inferred from the μT probe is stronger.

The entire set of the 72′674 individual dissipation values are compared in the histograms of Fig. 5. The two distributions do not follow lognormal (Monin and Yaglom, 1967; Baker and Gibson, 1987; Yamazaki and Lueck, 1990) or cut-lognormal (Davis,

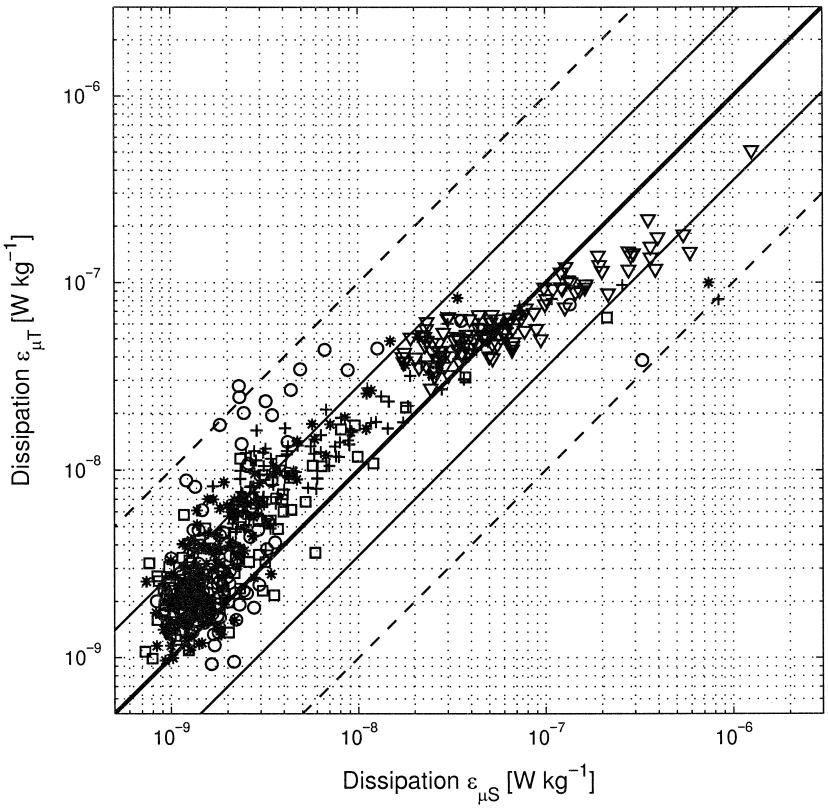

Fig. 6. Depth-averaged (segments of 0.25 m) dissipation $\varepsilon_{\mu T}$ and $\varepsilon_{\mu S}$ profiles for the five regimes (defined in Table 1) plotted against each other. Since dissipation increases towards the surface, the largest values for each regime represent the uppermost data. The straight lines represent perfect correspondence (bold), deviation by factors 2.8 ($=(2^2+2^2)^{1/2}$; light line) and 10 (dashed line), respectively.

1996) forms, since the atmospheric forcing is obviously not steady (Fig. 3). It is interesting to mention, that the subset of the ε values obtained under strong wind (regime W) follows a lognormal histogram (Fig. 5) with a peak at $\approx 10^{-8}$ W kg^{-1} and a standard deviation (intermittency factor) of $\sigma_{\ln(\varepsilon)} = 1.75$. Even though the wind-dominated subset has a lognormal distribution, one can not conclude that it represents homogeneous turbulence, which is necessary (but not sufficient) for lognormality. The large width of the histograms demonstrates that arithmetic averages are dominated by small numbers of large ε values. The overall averages $\langle \varepsilon_{\mu T} \rangle = 2.0 \times 10^{-8}$ W kg^{-1} and $\langle \varepsilon_{\mu S} \rangle = 1.7 \times 10^{-8}$ W kg^{-1} agree within the systematic uncertainties on a significance level of 95% according to the Student's *t*-test.

The histograms reveal that also the distributions of the ε values determined by the two different methods match quite well. Nevertheless, again three discrepancies become apparent: While ε values larger than 10^{-6} W kg^{-1} occur almost only for $\varepsilon_{\mu S}$, $\varepsilon_{\mu T}$ values are more frequent around 10^{-8} W kg^{-1} and below 6×10^{-11} W kg^{-1}.

After comparing the entire data set, we concentrate on depth-averaged vertical profiles for the five different regimes (Table 1). This differentiation allows the comparison of the two methods for five subsets, reflecting different forcing and turbulence levels. In addition depth-averaged profiles (containing subsets of 77–138 microstructure casts, Table 1) are less sensitive to intermittency (typically eight times less than the values contoured in Fig. 4). The five profiles, averaged for both microstructure methods are plotted vs. each other in Fig. 6. The lines are guides to the eyes and represent ratios between $\varepsilon_{\mu S}$ and $\varepsilon_{\mu T}$ values of 1:1 (bold); 1:2.8 (light) and 1:10 (dashed), respectively, and vice versa. The value $2.8 = (2^2 + 2^2)^{1/2}$ can be considered as the typical uncertainty of the ratio of the two estimates, assuming that both methods are uncertain within a factor of 2.

The ε values form two clouds: The bulk of the depth-averages falls into the interval 10^{-9} to 3×10^{-9} W kg^{-1}. Under conditions of strong wind (regime W), dissipation values center above 2×10^{-8} W kg^{-1}. The largest ε values for each of the five regimes corresponds to the uppermost estimate, since turbulence increases towards the surface. Most of the depth-averaged dissipation values coincide within a factor of 2.8 over the entire ε range. However it

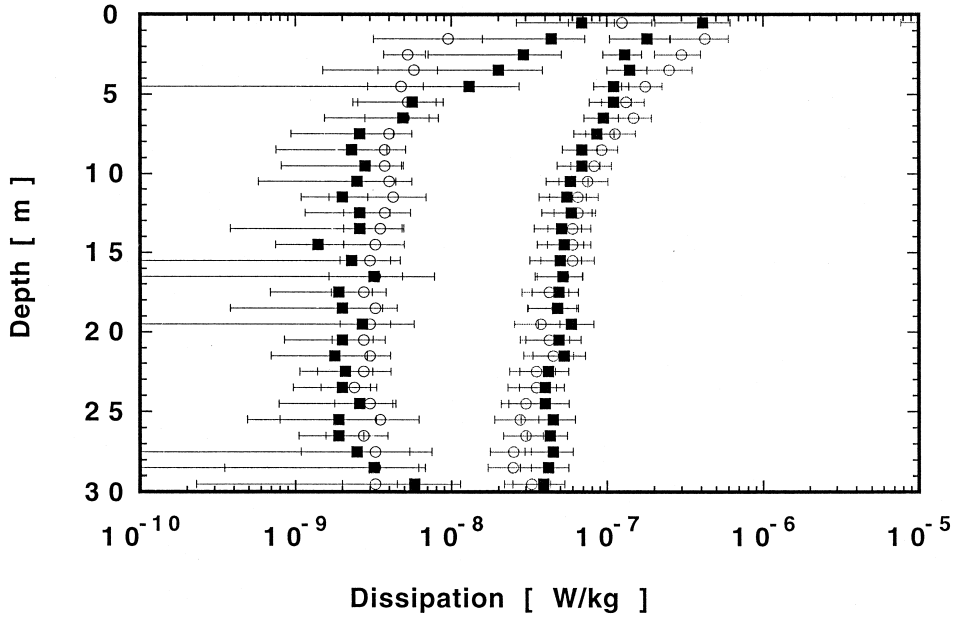

Fig. 7. Depth-averaged (segments of 1 m) dissipation $\varepsilon_{\mu T}$ (□) and $\varepsilon_{\mu S}$ profiles (○) for the regimes W (strong wind; right) and SH (strong heating; left), respectively. The error bars indicate bootstrap confidence level of 95%.

appears that the $\varepsilon_{\mu S}$ vs. $\varepsilon_{\mu T}$ plot shows some systematic deviations: Below 5×10^{-8} W kg^{-1} the $\varepsilon_{\mu T}$ values tend to be larger than the $\varepsilon_{\mu S}$ estimates, while above 10^{-7} W kg^{-1} the ratio between $\varepsilon_{\mu T}$ and $\varepsilon_{\mu S}$ follows a power law with exponent $1/2$. Most of the depth-averaged ε pairs, lying outside the factor 2.8 line, have two origins: They stem (1) from the top (wave-affected) surface layer under strong wind (regime W) and (2) from the depth range of about 1–4 m under strong heating (regime SH).

In the last step, we quantify the significance of the agreement of depth-averaged profiles. First, we compare the mean values, averaged over 0.25-m vertical segments. The Student's *t*-test turns out, that the hypothesis of identical mean values is accepted in all the depth segments at a significance level of more than 80% except the uppermost 0.75 m (three averages). The depth-averaged profiles of the two regimes, where deviations were apparently detected (see above), are compared in Fig. 7. Under strong wind (regime W), the $\varepsilon_{\mu T}$ and the $\varepsilon_{\mu S}$ profiles match very well, except in the top 3 m, where the deviation is slightly larger than the 95% bootstrap confidence level. For the regime of strong heating (regime SH), the agreement is again very well, except between 1 and 4 m depth, where the 95% bootstrap confidence level, however, is very broad due to the limited number of estimates (Table 1). Overall, the agreement of the depth-averaged ε estimates is well within the statistical boundaries except in the uppermost 1 m under strong wind (Fig. 7).

5. Discussion of the deviations

The good agreement between the $\varepsilon_{\mu S}$ and the $\varepsilon_{\mu T}$ values is documented in Figs. 4–7. Therefore, we concentrate in this section only on the deviations found by the statistical investigation. We identified two subsets, for which the ε values of the two methods are inconsistent at a significance level of 5%. These two subsets are: (1) Three averages (top 0.75 m) during the period of strong wind (regime W), where $\varepsilon_{\mu S} > \varepsilon_{\mu T}$ and (2) five averages (in the range of 1–4 m depth) during the period of strong heating (regime SH), where $\varepsilon_{\mu T} > \varepsilon_{\mu S}$. The third apparent deviation detected in Fig. 4, i.e., the enhanced values of $\varepsilon_{\mu T}$ during stratification (after March 17) in 15–20 m depth turned out not to be statistically significant. Hence, we consider only the deviations of subsets (1) and (2).

The deviations in subset (1), are most probably due to technical and methodological causes. Vibrations in the μS profiler caused by surface waves (especially regime W), reduce the number of 'good' estimates of $\varepsilon_{\mu S}$ in the uppermost surface layer. Consequently the 95% bootstrap confidence level of those depth-averages are very large (Fig. 7) and dominated by intermittency and not by the measurement uncertainty.

Another reason for $\varepsilon_{\mu S} > \varepsilon_{\mu T}$ is linked to the speed of the temperature microstructure profiler ($w = 0.08$ m s^{-1}). Since the sensor moves slowly compared to the horizontal phase speed c of the surface gravity waves ($c \approx 3$ m s$^{-1} \gg w$; Simon et al., 1999), the wave passes the μT profiler faster than the probe rises through the waves. As a result, the μT probe will hit the water surface close to the trough of the waves, whereas the μS profiler (rising five times faster) can rise also close to the crest of the waves, before hitting the surface. The vertical distance of the surface hit between the two methods can result in a difference of up to $\Delta z \approx 0.6$ m during strong wind. Consequently, the strong turbulence in the wave-affected surface layer is not sensed by the μT probe and the depth scale of the μT profile is shifted virtually upward. Both effects lead to an underestimation of $\varepsilon_{\mu T}$. An even more important effect might be that the velocity, at which the temperature fluctuations were sampled, was not adequate. The temperature microstructure field passes the probe at a velocity which is larger than the speed of the microstructure profiler. Consequently the microstructure field is sampled at higher wavenumber and consequently the spectral content is underestimated. Assuming a speed of 2 cm s^{-1} of the water relative to the profiler would lead to an underestimation of a factor of ≈ 2.5. As discussed in Section 2, an underestimation of the response time constant τ_{Resp} would also give lower dissipation values at high ε. From all three arguments we have solide indications that under strong wind the μT method might underestimate ε. In the wave affected surface layer, we therefore trust the $\varepsilon_{\mu S}$ values more than the $\varepsilon_{\mu T}$ values.

For the deviations in subset (2), where $\varepsilon_{\mu T} > \varepsilon_{\mu S}$ (regime SH in 1–4 m depth) it is possible, that remnant non-turbulent structures (so-called 'fossil' features) may spuriously contribute to the temperature spectra at high wavenumber and thereby drive up $\varepsilon_{\mu T}$. However due to the effect of molecular heat diffusion, 'fossil' features have their spectral contributions at wavenumber lower than the Batchelor wavenumber (definition in Fig. 8a). Therefore, we can not convincingly explain why the μT method under the stratifying effect of strong heating yield larger dissipation than the μS method.

6. Summary

Two microstructure methods to determine the rate of dissipation of turbulent kinetic energy in stratified natural waters have been established in the past: The *dissipation method* is based on measured records of small-scale shear fluctuations, whereas the *Batchelor method* makes use of measured records of temperature fluctuations. Given the assumptions on turbulence at small scales, which are necessary for the application of the two methods, it was not certain that the two methods would yield the same values of dissipation estimates. The reason for the small number of previous comparisons of the two methods is mainly due to the fact that shear profiler (using the μS method) are usually applied at a speed (typically ≈ 1 m s^{-1}), which does not enable the analysis of the high wavenumber end of the temperature spectra (response time too long). Criticism of the *Batchelor method* such as the uncertainty and non-constancy of the turbulence parameter q was the motivation for the presented comparison between the two methods.

The comparison is based on 826 temperature and shear microstructure profiles, measured simultaneously during an 12-day experiment conducted during March 1996 in the surface layer of Lake Neuchâtel (Switzerland). The μT and μS profilers, horizontally 35 m apart, were run upward at speeds of 0.08 and 0.35 m s^{-1}, respectively. During the experiment, the atmospheric forcing changed significantly leading to a range of hydrodynamic conditions (calm, windy, thermal convection, thermal stratification). These changing external conditions together with turbulence's inherent intermittency let the 72′674 individual dissipation estimates vary over six orders of magnitude from 10^{-11} to 10^{-5} W kg^{-1}. Based on the scaling relations for wind- and convectively-driven turbulence (Lombardo and Gregg, 1989), wind was the dominant forcing for turbulence in the surface boundary layer during most of the time. Convection was the dominant forcing for turbulence only during three nights.

The comparison revealed good agreement for the bulk of the estimates, with deviations being smaller than the assumed potential systematic bias of a factor of 2 between the two methods. Only two subsets, representing a very small portion of the data, showed systematic deviations larger than expected due to intermittency and statistics: (1) Under strong wind, the $\varepsilon_{\mu T}$ values were most probably underestimated due to the neglect of in situ currents, which affected the microstructure spectra seen by the rising temperature sensor. Additional uncertainties may come from incorrect time response correction for high $\varepsilon_{\mu T}$ values. We conclude that the dissipation method is superior under such conditions. The profiler vibrations are, however, a potential disadvantage of the shear measurements, especially within the wave-affected surface layer.

During strong heating depth-averaged $\varepsilon_{\mu T}$ estimates in the depth range of 1–4 m were found to exceed the $\varepsilon_{\mu S}$ estimates by up to a factor of 6. The reason for this discrepancy remains unclear, though we suspect stratification to be the responsible factor.

Taking into account the wide range of dissipation found and the intermittent character of turbulence, the observed agreement is very good. Both microstructure methods yield nearly the same dissipation values and we could not find a clear superiority of one over the other. Limitations of the Batchelor method (spatial resolution of temperature profile, low profiler velocity) do not allow estimation of dissipation above 10^{-5} W kg^{-1}. At very low turbulence, however, the μT method is less sensitive to profiler vibration than the μS method and enables dissipation estimates below 10^{-11} W kg^{-1}.

Acknowledgements

We wish to thank Bjarke Rasmussen, Peter Keller, Alexander Pufahl, Ulisse Devisioni and almost the

entire department of Environmental Physics at EAWAG for the support during the extensive field work. We especially thank Mike Schurter for the large number of moorings and time spent during data collection. Tom Osborn, Rolf Lueck and two anonymous reviewers made helpful comments for improving the manuscript. The English was polished by Tom Ravens. This study was supported by Swiss National Science Foundation grants 20-36364.92, 20-43357.95 and 20-50761.97.

Appendix A

A.1. Details of the Batchelor (temperature microstructure) method

The microstructure temperature (range: -3 to 30°C) was measured with a FP07 thermistor (Thermometrics, USA) and digitized with a 16-bit A/D converter. Since the resolution of the thermistor is better than the bit resolution $\Delta^2/12 = 2.1 \times 10^{-8}$ K^2 (Proakis and Manolakis, 1988) and since geophysical temperature signals show usually red spectra, the noise due to the bit resolution is reduced by preemphasing the signal prior to A/D conversion according to

$$H(\omega) = \frac{1 + i\tau_1\left(l + \dfrac{\tau_2}{\tau_1}\right)\omega}{1 + i\tau_2\,\omega} \qquad [-] \qquad (A.1)$$

as a function of the frequency ω, with the time constants $\tau_1 = 1.576$ s and $\tau_2 = 0.787 \times 10^{-3}$ s (Seabird, 1990). After A/D conversion, the preemphasis is reversed by deemphasising the signal numerically. This pre-/deemphasis procedure (Mudge and Lueck, 1994) reduces digitization noise by the factor $|H(\omega)|^{-2}$ and as a result, high frequency temperature fluctuations are extremely well resolved (Fig. 8a).

For the calculation of the spectra temperature data were first detrended. To reduce the variation of the estimated power spectrum the Welsh method was used with non-overlapping segments and the Hanning window to smooth the edges of the data window (Press et al., 1986; Percival and Walden, 1993). The limited response time τ_{Resp} of the thermistor (Section 2) damps the temperature fluctuations in the high wavenumber range. To compensate for this reduction, the measured spectrum $\phi_{\mathrm{T}}^{\mathrm{m}}$ was multiplied by $(1 + w^2 k_z^2 \tau_{\mathrm{Resp}}^2)$. This implies, that Taylor hypothesis was used for the conversion from frequencies into wave numbers (= profiler speed).

The wavenumber at which the temperature signal reaches the noise level (Fig. 8a), determines the upper limit of the resolution of the temperature spectra. The noise spectrum was estimated experimentally isolating the thermistor by a cap. The fit of the measured spectra to the Batchelor spectra (Eq. (2)) was applied only to the spectral content below that upper boundary. Noise level detection, necessary for fitting worked automatically for more than 97% of the segments.

The dissipation of temperature variance χ was determined by two different ways. $\chi_{\mathrm{Batchelor}}$ (and $\varepsilon_{\mu\mathrm{T}}$) was estimated by fitting the corrected measured spectra to the model spectrum (Eq. (2)). As a fit quality criterion we compared $\chi_{\mathrm{Batchelor}}$ with χ_{Int}, which was calculated by integrating the temperature spectrum according to:

$$\chi_{\mathrm{Int}} = 12\kappa \int_0^{\infty} k_z^2 \phi_{\mathrm{T}}\,\mathrm{d}k_z \qquad [\mathrm{K}^2\ \mathrm{s}^{-1}] \qquad (A.2)$$

The lower and upper limit of the estimation of dissipation ε is also demonstrated in Fig. 8a. The shown spectra (from field data), correspond to dissipation values from $\varepsilon = 6 \times 10^{-13}$ to $\varepsilon = 7.5 \times 10^{-6}$

Fig. 8. (a) Comparison of two in situ temperature spectra with the noise level (triangles) determined in the field with the cap-covered thermistor (noise from sensor and electronics only). (*): Spectrum from 400 m depth in Lake Baikal (Kocsis et al., 1999). The spectrum is still more than 2 orders of magnitude above the noise level, even though $\varepsilon_{\mu\mathrm{T}} = 6.0 \times 10^{-13}$ W kg^{-1} and $\chi = 1.0 \times 10^{-12}$ K^2 s^{-1} are extremely small. (○): Spectrum with the highest $\varepsilon_{\mu\mathrm{T}}$ estimate ($\varepsilon_{\mu\mathrm{T}} = 7.5 \times 10^{-6}$ W kg^{-1}; $\chi = 1.6 \times 10^{-5}$ K^2 s^{-1}) determined in the surface layer of Lake Neuchâtel (this study). For such a $\varepsilon_{\mu\mathrm{T}}$ value still 92% of the temperature fluctuations are resolved (≈ upper limit of the μT method). The light vertical lines indicate the Batchelor wavenumbers $(2\pi)^{-1}(\varepsilon/\nu\kappa_{\mathrm{T}}^2)^{1/4}$ corresponding to the two spectra (○ and *). (b) Comparison of the dissipation of temperature variance χ obtained by fitting to the Batchelor spectra $\chi_{\mathrm{Batchelor}}$ (Eq. (2)) and by integration of the spectra χ_{Int} (Eq. (A.2)). The excellent correlation (lines mark deviation of factor 2) indicates that there are not systematic deviations from the Batchelor form as a function of χ.

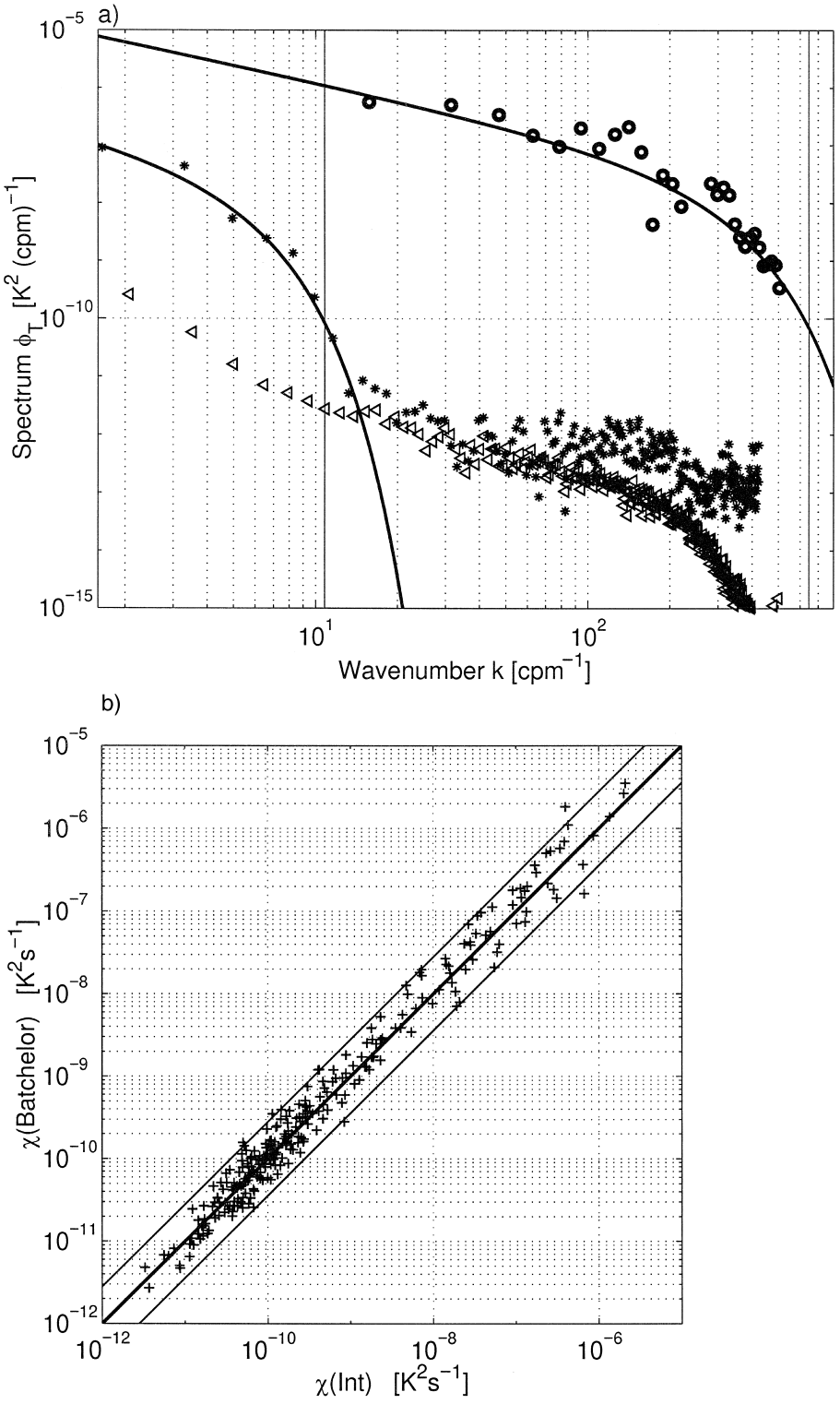
a)
Spectrum ϕ_T [K^2 (cpm)$^{-1}$]
Wavenumber k [cpm^{-1}]
b)
χ(Batchelor) [K^2s^{-1}]
χ(Int) [K^2s^{-1}]

W kg^{-1}. The lower limit of the ε estimate is determined by those spectra, which are still clearly above the noise level of the sensor. The upper limitation is given by the ability to resolve the shortest temperature fluctuations. For the given example ($\varepsilon = 7.5 \times 10^{-6}$ W kg^{-1}), the smallest length scale to be resolved, expressed by the Batchelor scale, is 1.6 mm and the necessary time constant of the sensor is $\tau = 20$ ms (1.6 mm/w). Therefore, the corresponding Batchelor model spectrum (Fig. 8a) is resolved to more than 92% of the temperature variance.

To check the quality of the fits to the Batchelor spectra, dissipation of temperature variance obtained by fitting $\chi_{\text{Batchelor}}$ (Eq. (2)) and by integration of the spectra χ_{Int} (Eq. (A.2)) are compared in Fig. 8b. The histogram of the logarithmic ratio $\log_{10}(\chi_{\text{Batchelor}}/\chi_{\text{Int}})$ for profiles from this study shows a symmetric distribution around zero, with a mean value $\langle(\chi_{\text{Batchelor}}/\chi_{\text{Int}})\rangle = 1.2$ and a standard deviation $\sigma(\log(\chi_{\text{Batchelor}}/\chi_{\text{Int}})) = 0.47$. The agreement between the fitted $\chi_{\text{Batchelor}}$ and the integrated χ_{Int} values over many orders of magnitude without any trend, reveals, that the approximation of the Batchelor spectra is very good and independent of the intensity of turbulence and the temperature background gradient. This good correspondence is even more remarkable, since the χ values show stronger intermittency than the dissipation ε (Davis, 1993, 1994).

A.2. Technical details to the PNS 93 shear sensor

PNS 93 shear probe consists of an axially symmetric airfoil separated by a cantilever from a piezoceramic beam (Fig. 9). The length and diameter of the airfoil are 3.5 mm and 3 mm, respectively. The piezoceramic beam as well as the cantilever are protected by a cone-shaped metallic cap. Only the airfoil stands out from the cap. The narrow gap between cantilever and cap prevents damage to the beam by strong bending. During in situ operations, the interior of the cap is water filled. The PNS 93 shear probe has a narrow band resonance peak at 315 Hz. In the frequency range below 270 Hz no systematic frequency-dependent sensor output occurs (Prandke, 1994).

The general behavior of airfoil sensors have been described in detail by Osborn and Crawford (1980). The mean velocity due to the profiling speed of the probe is aligned with the axis of the probe. While the probe is not sensitive to axial forces, the cross-stream (transverse) components of turbulent velocity produce a lift force at the airfoil, sensed by the piezoceramic beam. The voltage output of the piezoceramic element, proportional to the instantaneous cross-stream component of the velocity field, is amplified and high-pass filtered. The high-pass with a slope of 6 dB/octave (20 dB/decade) and a time constant of 1 s acts as a differentiator for the sensor signal.

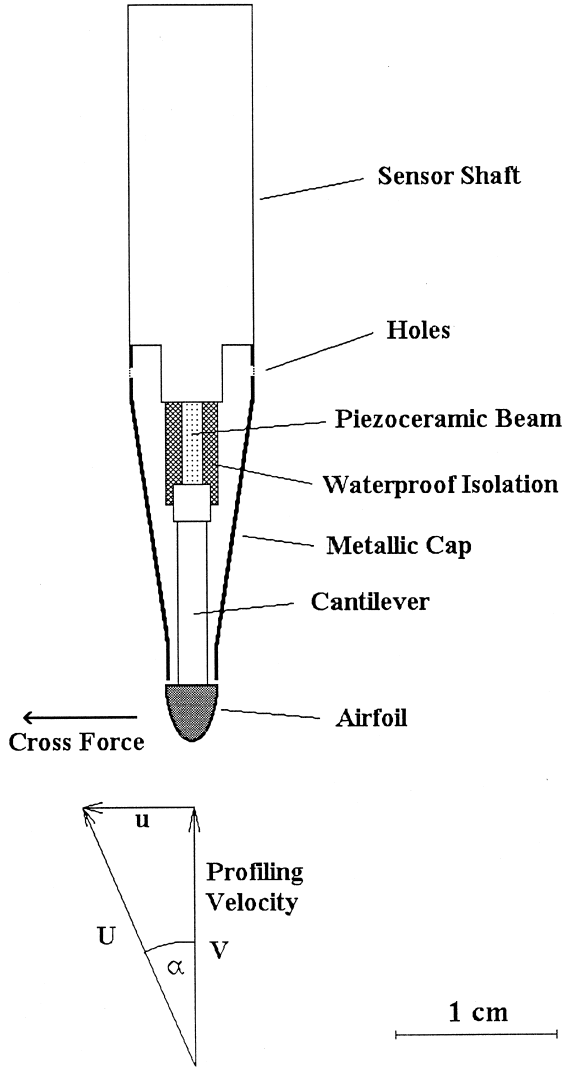

Fig. 9. Construction of the PNS 93 shear probe with schematic flow geometry. The airfoil and the piezoceramic beam are separated by a cantilever. The length and diameter of the airfoil are 3.5 mm and 3 mm, respectively.

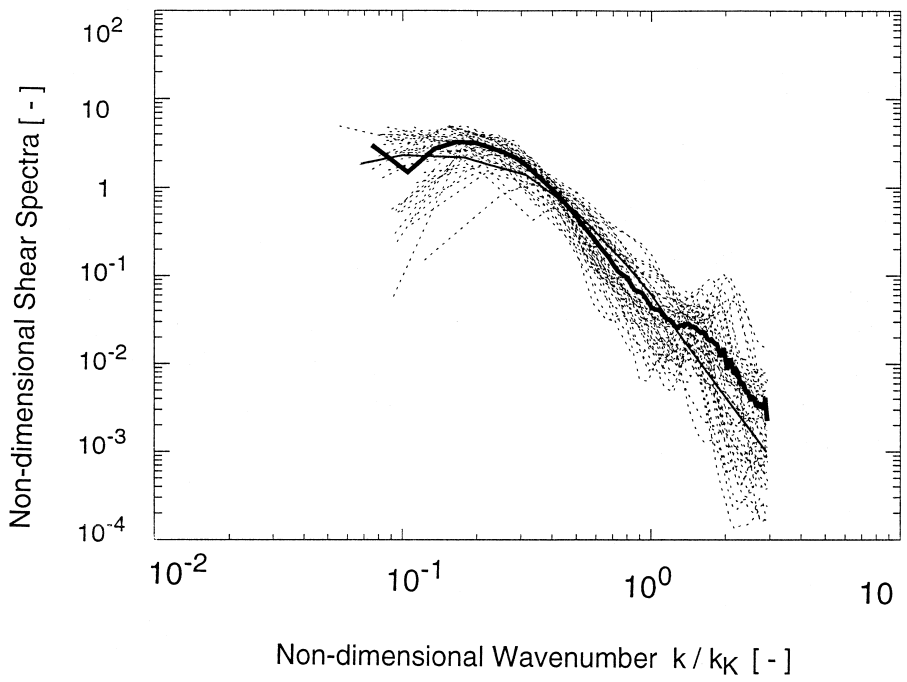

Fig. 10. 55 Non-dimensional spectra, measured with the of PNS 93 shear probe in the surface layer of Lake Neuchâtel, compared in an overlay plot with the spectra average (bold) and the Nasmyth spectrum (thin). The systematic deviations of the raw shear at large wavenumbers are not of interest, as they are above the range of significant contributions to the variance. For definition of the non-dimensional spectrum, see Oakey (1982).

Finally, a 500 Hz low-pass acts as an anti-aliasing filter. While the probe construction allows immediate response, the electronics gives the sensor a response time in the order of 1 ms.

Calibration of the PNS 93 shear probes was performed in the laboratory of ME Meerestechnik-Elektronik according to the arrangement by Osborn and Crawford (1980). The probe rotates about its axis of symmetry at 1 Hz under an angle of attack in a water jet. As the probe rotates in the jet, the total cross-force on the probe remains constant but the force on the piezoceramic beam varies sinusoidally. At a constant jet velocity U, the rms voltage output of the probe E_{rms} is measured at different angles of attack between 0 and 10 degree. The probe sensitivity S is the slope of the regression (best fit of a cubic approximation) of $E_{\mathrm{rms}}/(\rho U^2)$ vs. $\sin 2\alpha$ at $\alpha = 0°$. The PNS 93 shear probe data processing is based on the potential flow theory (Allen and Perkins, 1952). Details on the data analysis are given in Prandke and Stips (1998). Shear spectra measured in the field are shown in Fig. 10, where 55 spectra of raw shear are overlaid, which stem from a randomly selected profile collected in the top 15 m of Lake Neuchâtel during this study.

References

Allen, H.J., Perkins, E.W., 1952. A study of effects of flow over slender inclined bodies of revolution. Report No. 1048, U.S. National Advisory Committee for Aeronautics.

Baker, M.A., Gibson, C.M., 1987. Sampling turbulence in the stratified ocean: statistical consequences of strong intermittency. J. Phys. Oceanogr. 17, 1817–1836.

Batchelor, G.K., 1959. Small-scale variation of convected quantities like temperature in turbulent fluid: Part 1. General discussion and the case of small conductivity. J. Fluid. Mech. 5, 113–133.

Davis, R.E., 1993. Diapycnal mixing in the ocean: equations for large-scale budgets. J. Phys. Oceanogr. 24, 777–800.

Davis, R.E., 1994. Diapycnal mixing in the ocean: the Osborn–Cox model. J. Phys. Oceanogr. 24, 2560–2576.

Davis, R.E., 1996. Sampling turbulent dissipation. J. Phys. Oceanogr. 26, 341–358.

Dillon, T.M., Caldwell, D.R., 1980. The Batchelor spectrum and

dissipation in the upper ocean. J. Geophys. Res. 85, 1910–1916.
Gargett, A.E., 1985. Evolution of scalar spectra with the decay of turbulence in a stratified fluid. J. Fluid Mech. 159, 379–407.
Gibson, C.H., Schwarz, W.H., 1963. The universal equilibrium spectra of turbulent velocity and scalar fields. J. Fluid Mech. 16, 365–384.
Gloor, M., Kocsis, O., Omlin, M., Schurter, M., Wüest, A., 1995. Temperaturmikrostrukturen, eine Methode zur Bestimmung der Mischungsintensität in geschichteten Gewässern. Gas Wasser Abwasser 75, 1087–1096.
Goudsmit, G.H., Peeters, F., Gloor, M., Wüest, A., 1997. Boundary versus internal diapycnal mixing in stratified natural waters. J. Geophys. Res. 102, 27903–27914.
Grant, H.L., Hughes, B.A., Vogel, W.M., Moilliet, A., 1968. The spectrum of temperature fluctuations in turbulent flow. J. Fluid Mech. 34, 423–442.
Gregg, M.C., 1989. Scaling turbulent dissipation in the thermocline. J. Geophys. Res. 94, 9686–9698.
Gregg, M.C., 1991. The study of mixing in the ocean: a brief history. Oceanography, April, p. 39–45.
Gregg, M.C., Meagher, T., 1980. The dynamic response of glass rod thermistors. J. Geophys Res. 85, 2779–2786.
Imberger, J., Boashash, B., 1986. Application of the Wigner–Ville distribution to temperature gradient microstructure: a new technique to study small-scale variations. J. Phys. Oceanogr. 16, 1997–2012.
Kocsis, O., Ravens, T., Granin, N., Wüest, A., 1999. Turbulence and diapycnal diffusivity in the stratified deep water of the South Basin of Lake Baikal. Limnol. Oceanogr., in review.
Ledwell, J.R., Watson, A.J., Law, C.S., 1993. Evidence for slow mixing across the pycnocline from an open-ocean tracer-release experiment. Nature 364, 701–703.
Lombardo, C.P., Gregg, M.C., 1989. Similarity scaling of viscous and thermal dissipation in a convecting surface boundary layer. J. Geophys. Res. 94, 6273–6284.
Monin, A.S., Yaglom, A.M., 1967. Statistical Fluid Mechanics, Vol. 1. The MIT Press.
Moum, J.N., Gregg, M.C., Lien, R.C., Carr, M.E., 1995. Comparison of turbulence kinetic energy dissipation rate estimates from two ocean microstructure profilers. J. Atmos. Oceanic Technol. 12, 346–366.
Mudge, T.D., Lueck, R.G., 1994. Digital signal processing to enhance oceanographic observations. J. Atmos. Oceanic Technol. 11, 825–836.
Oakey, N.S., 1982. Determination of the rate of dissipation of turbulent energy from simultaneous temperature and velocity shear microstructure measurements. J. Phys. Oceanogr. 12, 256–271.
Osborn, T.R., 1980. Estimates of the local rate of vertical diffusion from dissipation measurements. J. Phys. Oceanogr. 10, 83–89.
Osborn, T.R., Crawford, W.R., 1980. An airfoil probe for measuring turbulent velocity fluctuations in water. In: Dobson, F., Hasse, L., David, R. (Eds.), Air–Sea Interaction: Instruments and Methods, Chap. 19. Plenum, New York, pp. 369–386.
Percival, D.B., Walden, A.T., 1993. Spectral Analysis for Physical Applications. Cambridge Univ. Press, Cambridge.
Peters, H., Gregg, M.C., Toole, J.M., 1988. On the parameterization of equatorial turbulence. J. Geophys. Res. 93, 1199–1218.
Prandke, H., 1994. Tests and intercalibrations of an improved airfoil shear probe. ME Meerestechnik-Elektronik, Trappenkamp, Technical Report, April 1994.
Prandke, H., Stips, A., 1996. Investigation of microstructure and turbulence in marine and limnic waters using the MST Profiler. Technical Note No. I.96.87, European Commission, Joint Research Centre, Space Applications Institute, Ispra/Italy.
Prandke, H., Stips, A., 1998. Test measurements with an operational microstructure-turbulence profiler: detection limit of dissipation rates. Aquat. Sci. 60, 191–209.
Press, W.H., Flannery, B.P., Teukolsky, S.A., Vetterling, T.W., 1986. Numerical Recipes. Cambridge Univ. Press, Cambridge.
Proakis, J.G., Manolakis, D.G., 1988. Introduction to Digital Signal Processing. MacMillan, New York.
Sander, J., 1998. Dynamical equations and turbulent closures in geophysics. Continuum Mech. Thermodyn. 10, 1–28.
Seabird, 1990. Technical Manual for Temperature-Microstructure Probe SBE-11.
Sherman, J.T., Davis, R.E., 1995. Observations of temperature microstructure in NATRE. J. Phys. Oceanogr. 25, 1913–1929.
Simon, A., 1997. Turbulent mixing in the surface boundary layer of lakes. Diss. ETH Nr. 12272. p. 99.
Simon, A., Stips, A., Kocsis, O., Wüest, A., 1999. Momentum and turbulent kinetic energy balance in the surface boundary layer in the presence of underdeveloped waves. In prep.
Vachon, P., Lueck, R.G., 1984. A small combined temperature and conductivity probe. Proceedings of the 1984 STD Conference and Workshop, sponsored by the Marine Technology Society and the MPS Oceanic Instrumentation Committee, San Diego.
Walraven, R., 1984. Digital filters. Proceedings of Digital Equipment User's Society, Fall, 1984, Department of Applied Sciences, University of California, Davies, CA.
Wüest, A., Van Senden, D.C., Imberger, J., Piepke, G., Gloor, M., 1996. Comparison of diapycnal diffusivities measured by tracer and microstructure techniques. Dyn. Atmos. Oceans 24, 27–39.
Yamazaki, H., Lueck, R., 1990. Why oceanic dissipation rates are not lognormal. J. Phys. Oceanogr. 20, 1907–1918.